The Journal of Chemical Physics

RESEARCH ARTICLE | JANUARY 19 2022

Construction of meta-GGA functionals through restoration of exact constraint adherence to regularized SCAN functionals FREE

James W. Furness ; Aaron D. Kaplan ; Jinliang Ning ; John P. Perdew ; Jianwei Sun

J. Chem. Phys. 156, 034109 (2022)
https://doi.org/10.1063/5.0073623
CHORUS

AIP Publishing

The Journal of Chemical Physics ARTICLE scitation.org/journal/jcp

Construction of meta-GGA functionals through restoration of exact constraint adherence to regularized SCAN functionals

Cite as: J. Chem. Phys. 156, 034109 (2022); doi: 10.1063/5.0073623
Submitted: 1 October 2021 • Accepted: 21 December 2021 •
Published Online: 19 January 2022

James W. Furness,[1,a] Aaron D. Kaplan,[2,b] Jinliang Ning,[1] John P. Perdew,[2,3,c] and Jianwei Sun[1,d]

AFFILIATIONS

[1] Department of Physics and Engineering Physics, Tulane University, New Orleans, Louisiana 70118, USA
[2] Department of Physics, Temple University, Philadelphia, Pennsylvania 19122, USA
[3] Department of Chemistry, Temple University, Philadelphia, Pennsylvania 19122, USA

[a] jfurness@tulane.edu
[b] Author to whom correspondence should be addressed: kaplan@temple.edu
[c] perdew@temple.edu
[d] jsun@tulane.edu

ABSTRACT

The strongly constrained and appropriately normed (SCAN) meta-GGA exchange–correlation functional [Sun *et al.*, Phys. Rev. Lett. **115**, 036402 (2015)] is constructed as a chemical environment-determined interpolation between two separate energy densities: one describes single-orbital electron densities accurately and another describes slowly varying densities accurately. To conserve constraints known for the exact exchange–correlation functional, the derivatives of this interpolation vanish in the slowly varying limit. While theoretically convenient, this choice introduces numerical challenges that degrade the functional's efficiency. We have recently reported a modification to the SCAN meta-GGA, termed restored-regularized-SCAN (r^2SCAN) [Furness *et al.*, J. Phys. Chem. Lett. **11**, 8208 (2020)], that introduces two regularizations into SCAN, which improve its numerical performance at the expense of not recovering the fourth order term of the slowly varying density gradient expansion for exchange. Here, we show the derivation of a progression of density functional approximations [regularized SCAN (rSCAN), r++SCAN, r^2SCAN, and r^4SCAN] with increasing adherence to exact conditions while maintaining a smooth interpolation. The greater smoothness of r^2SCAN seems to lead to better general accuracy than the additional exact constraint of SCAN or r^4SCAN does.

I. INTRODUCTION

The importance of efficient computational modeling in chemistry and materials science cannot be understated, and for many applications, Kohn–Sham density functional theory presents the most appealing compromise between accuracy and efficiency. The favorable position of this compromise has been enabled by the steady progression of ever more accurate density functional approximations (DFAs) produced over the last 60 years. These DFAs are commonly characterized by the Perdew–Schmidt hierarchy,[1] a progression of increasing non-locality where successive levels can be expected to give greater accuracy at the cost of increased computational complexity.

The meta-generalized gradient approximations (meta-GGAs) stand as an appealing level at which the highest accuracy can be expected from semi-local ingredients, including the electron density, its gradient, its Laplacian, and the kinetic energy density. This article focuses on meta-GGAs that do not depend on the Laplacian of the density. While hybrid functionals incorporating admixtures of nonlocal single-determinant exchange have become most prominent for molecular applications, the prohibitive cost scaling of nonlocal exchange with the number of electrons has limited their utility for extended systems.

A meta-GGA is commonly designed either by enforcing constraints on the exchange–correlation (XC) functional or by fitting to reference datasets. Those that take the latter route, called

empirical DFAs, can be inaccurate for systems outside their respective fitting set or can suffer from difficulties due to over-fitting. General purpose DFAs that are accurate for diverse systems have tended to be of the former, so-called non-empirical, variety in which transferable accuracy is promoted by adherence to physical constraints that are necessarily true for all systems of electrons. The first generation of meta-GGAs was non-empirical and predated most GGAs. Becke and Roussel[2,3] derived generalized Taylor series of the exact exchange hole by enforcing sum rule and non-positivity constraints on a hole model. Perdew[4] derived a Laplacian-level meta-GGA for the exchange energy by enforcing the same set of constraints.

At the meta-GGA level, the strongly constrained and appropriately normed (SCAN) functional has incorporated all 17 known

TABLE I. Accuracy for appropriate norms. Rare gas atom exchange–correlation energies are given in hartrees (E_h), jellium surface exchange–correlation formation energies are given in erg/cm^2, and Ar_2 interaction energies are given in kcal/mol. Benchmark data for rare gas atom exchange–correlation, jellium surface exchange–correlation, and Ar_2 interaction energy are from Refs. 77–80 and 82, respectively. Error summaries are given as mean absolute percentage errors (MAPEs). Full calculation details are in the main text.

		SCAN (%)	rSCAN (%)	r++SCAN (%)	r^{2}SCAN (%)	r^{4}SCAN (%)	Benchmarks
Ne	E_x	−12.164(0.48)	−12.183(0.64)	−12.176(0.58)	−12.144(0.32)	−12.146(0.34)	−12.105 E_h
	E_c	−0.345(−11.81)	−0.346(−11.53)	−0.347(−11.36)	−0.347(−11.24)	−0.347(−11.24)	−0.391 E_h
	E_{xc}	−12.508(0.10)	−12.529(0.26)	−12.522(0.21)	−12.491(−0.04)	−12.493(−0.03)	−12.496 E_h
Ar	E_x	−30.264(0.29)	−30.295(0.40)	−30.281(0.35)	−30.182(0.02)	−30.196(0.07)	−30.175 E_h
	E_c	−0.690(−4.81)	−0.695(−4.24)	−0.696(−4.06)	−0.697(−3.90)	−0.697(−3.90)	−0.725 E_h
	E_{xc}	−30.955(0.17)	−30.990(0.29)	−30.977(0.25)	−30.879(−0.07)	−30.893(−0.02)	−30.901 E_h
Kr	E_x	−94.071(0.25)	−94.215(0.41)	−94.186(0.37)	−93.820(−0.02)	−93.940(0.11)	−93.834 E_h
	E_c	−1.756(−5.10)	−1.765(−4.59)	−1.768(−4.47)	−1.770(−4.34)	−1.770(−4.34)	−1.850 E_h
	E_{xc}	−95.827(0.15)	−95.980(0.31)	−95.953(0.28)	−95.590(−0.10)	−95.710(0.03)	−95.684 E_h
Xe	E_x	−179.315(0.14)	−179.614(0.31)	−179.567(0.28)	−178.827(−0.13)	−179.136(0.04)	−179.064 E_h
	E_c	−2.899(−3.43)	−2.910(−3.07)	−2.914(−2.96)	−2.918(−2.82)	−2.918(−2.82)	−3.002 E_h
	E_{xc}	−182.214(0.08)	−182.524(0.25)	−182.480(0.23)	−181.745(−0.18)	−182.053(−0.01)	−182.066 E_h
MAPE [E_x]		0.29	0.44	0.40	0.12	0.14	
MAPE [E_c]		6.29	5.86	5.71	5.58	5.58	
MAPE [E_{xc}]		0.13	0.28	0.24	0.10	0.02	
$r_s = 2$	E_x	2631.022(−0.27)	2198.716(16.21)	2259.204(13.90)	2318.763(11.63)	2419.739(7.78)	2624.000 erg/cm^2
	E_c	811.437(−5.66)	989.604(−28.85)	971.939(−26.55)	963.796(−25.49)	963.796(−25.49)	768.000 erg/cm^2
	E_{xc}	3442.459(−1.49)	3188.320(6.00)	3231.143(4.74)	3282.559(3.23)	3383.535(0.25)	3392.000 erg/cm^2
$r_s = 3$	E_x	489.080(7.02)	352.217(33.04)	394.134(25.07)	412.474(21.58)	424.755(19.25)	526.000 erg/cm^2
	E_c	299.340(−23.69)	361.776(−49.49)	342.788(−41.65)	339.987(−40.49)	339.987(−40.49)	242.000 erg/cm^2
	E_{xc}	788.419(−2.66)	713.992(7.03)	736.922(4.05)	752.461(2.02)	764.741(0.42)	768.000 erg/cm^2
$r_s = 4$	E_x	126.894(19.18)	82.262(47.60)	92.568(41.04)	100.800(35.80)	102.789(34.53)	157.000 erg/cm^2
	E_c	146.586(−40.95)	152.932(−47.05)	162.499(−56.25)	161.117(−54.92)	161.117(−54.92)	104.000 erg/cm^2
	E_{xc}	273.480(−4.78)	235.194(9.89)	255.068(2.27)	261.917(−0.35)	263.906(−1.11)	261.000 erg/cm^2
$r_s = 6$	E_x	6.264(71.53)	30.717(−39.62)	−1.577(107.17)	1.210(94.50)	1.604(92.71)	22.000 erg/cm^2
	E_c	52.651(−69.84)	20.481(33.93)	56.057(−80.83)	55.508(−79.06)	55.508(−79.06)	31.000 erg/cm^2
	E_{xc}	58.915(−11.16)	51.199(3.40)	54.480(−2.79)	56.719(−7.02)	57.112(−7.76)	53.000 erg/cm^2
MAPE [E_x]		24.50	34.12	46.79	40.88	38.57	
MAPE [E_c]		35.03	39.83	51.32	49.99	49.99	
MAPE [E_{xc}]		5.02	6.58	3.46	3.15	2.39	
Ar_2 1.6 Å		360.936(−1.19)	361.031(−1.17)	360.200(−1.39)	362.516(−0.76)	360.616(−1.28)	365.292 kcal/mol
Ar_2 1.8 Å		195.723(−1.28)	197.023(−0.62)	196.277(−1.00)	198.109(−0.07)	196.431(−0.92)	198.255 kcal/mol
Ar_2 2.0 Å		102.465(−0.73)	103.577(0.35)	102.889(−0.32)	104.242(1.00)	103.151(−0.06)	103.215 kcal/mol
MAPE		1.07	0.71	0.90	0.61	0.75	

constraints on the exact XC energy appropriate to the semi-local level.[5] (These constraints are listed together in the supplementary material of Ref. 5, and the references for them are presented in the main text of Ref. 5.) From this foundation, further works have proposed modifications to the SCAN energy densities to improve its accuracy in certain domains. revSCAN is a simple modification to the slowly varying limit of SCAN's correlation energy that modifies the fourth order term in its density gradient expansion.[6] The TASK meta-GGA is a complete revision of SCAN, retaining only its fulfillment of exact constraints for the exchange energy.[7] TASK is designed to accurately predict bandgaps and has recently been itself extended for accuracy in 2D systems, in a modification termed "mTASK."[8] Note that TASK and mTASK use a correlation DFA at the level of the local spin-density approximation (LSDA).

The SCAN meta-GGA has proved broadly transferable and has shown good accuracy for many systems normally challenging for DFT methods,[9–32] although its numerical difficulties have hindered some applications such as pseudo-potential generation.[33,34] To address this, Bartók and Yates[33] proposed a regularized SCAN, termed "rSCAN," that aims to control numerical challenges while remaining as close to the original SCAN meta-GGA as possible. While the regularizations are effective in improving numerical performance and removing the grid sensitivity of SCAN that is problematic in some electronic structure codes, they break five of the exact conditions SCAN was designed to obey. Recent work by Mejía-Rodríguez and Trickey shows that some transferability is lost in rSCAN, with atomization energies particularly degraded.[35,36] We have recently proposed a restored-regularized-SCAN, called r^{2}SCAN, which maintains the regularizations of rSCAN while restoring exact constraint adherence.[37]

Compared to SCAN, the resulting r^{2}SCAN meta-GGA has shown pronounced improvements in numerical efficiency, alongside small systematic improvements in accuracy.[31,37–41] Among the DFAs constructed to satisfy exact constraints without fitting to bonded systems, the strong improvements in predictive accuracy from LSDA to the Perdew–Burke–Ernzerhof (PBE) GGA[42] to the SCAN (or r^{2}SCAN) meta-GGA have been extensively documented.[5,9–41] Broad comparisons with other DFAs have also been reported for the extensive GMTKN55 test set[43] for main-group chemistry: the overall error measure WTMAD-2 was[40] 8.6 kcal/mol for SCAN + D4 and 7.5 kcal/mol for r^{2}SCAN + D4, where D4 is a dispersion correction. Applying SCAN + D4 to the unrestricted Hartree–Fock density[44] instead of its own self-consistent density leads to a remarkably small WTMAD-2 of 5.079 kcal/mol, better than nearly all the (necessarily empirical) hybrid functionals tested thus far. This "density correction"[45] to SCAN also leads to a nearly perfect many-body expansion and molecular dynamics for water.[46] In a test of the equilibrium properties (other than the fundamental bandgap) of important classes of solids,[47] SCAN was overall better than all other tested functionals, including a hybrid functional with non-local single-determinant exchange at short range.

The present publication completes Ref. 37, providing the necessary details of how each exact constraint was restored in r^{2}SCAN, and extends its analysis to a progression of regularized DFAs (rSCAN, r++SCAN, r^{2}SCAN, and r^{4}SCAN) that ultimately restore all the exact constraints obeyed by SCAN. We show how these restorations affect the numerical performance of the DFAs and how smoothness can be maintained for all constraints except the fourth order term of the slowly varying density gradient expansion for exchange, which is less easy to enforce following the present interpolation-based model. This work also provides context for the exact constraints enforced by SCAN and demonstrates how a meta-GGA can be constructed to enforce those constraints. We also include a more detailed analysis of the construction of r^{2}SCAN than was presented in Ref. 37: in addition to a derivation of the r^{2}SCAN gradient expansion in the supplementary material, Fig. 4 shows how the damping factor d_{p2} of r^{2}SCAN was determined.

This work also presents numerical results for all four regularized DFAs. We report individual errors on their appropriate norms (used to determine their parameters) in Table I and errors in the lattice constants of solids in Table IV and in those solids' corresponding bulk moduli in Tables V and S10. Figures 3 and 5–7 will be familiar to readers of Ref. 37 but are expanded to incorporate results for the new meta-GGAs. Variations of Figs. 1 and 2 were presented in Ref. 37; they are included here for completeness. The tables in Appendixes C–F of the supplementary material report results for the same test sets considered in Ref. 37, but including the novel meta-GGAs.

Before proceeding to the present work, it is worth discussing a specific approach within semi-empirical DFA design that is still relatively nascent. Machine-learning techniques have recently been used to self-consistently determine a SCAN-like meta-GGA that still satisfies some of the exact constraints of SCAN.[48] The history of machine learning in DFA design actually begins much earlier; however, these early works (e.g., Ref. 49) tended to apply machine-learning approaches to the exchange–correlation potential. The approach of Ref. 48 is also novel in its use of a self-consistency cycle to determine the performance of the functional for each possible parameter set. It should be noted that the functional of Ref. 48 was primarily fitted to properties of bonded systems, including atomization energies and chemical reaction barrier heights. Most empirical approaches, and the approach used here, evaluate the DFA

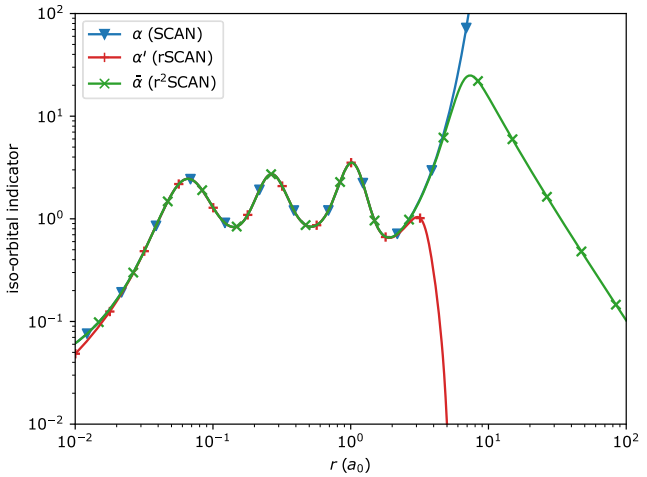

FIG. 1. Comparison between conventional α (e.g., from SCAN), α' (from rSCAN), and new $\bar{\alpha}$ as a function of distance from the Kr nucleus (in Bohr radii) computed from accurate spherical Hartree–Fock datasets with Slater-type orbitals.[67,68] Regularization parameters are $\tau_r = 10^{-4}$ and $\alpha_r = 10^{-3}$ in α' and $\eta = 10^{-3}$ in $\bar{\alpha}$.

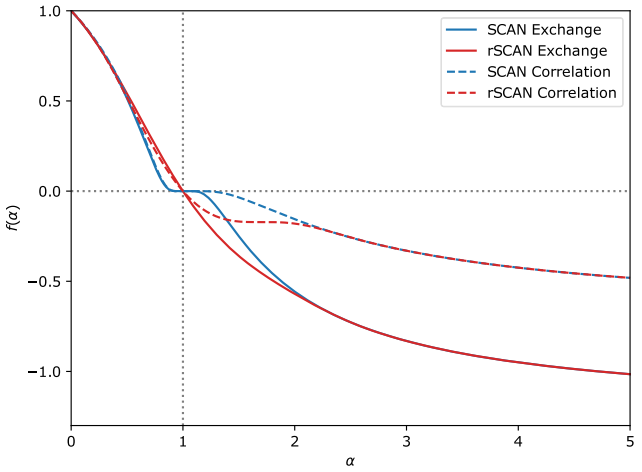

FIG. 2. The exchange (solid) and correlation (dashed) interpolation functions for the SCAN [blue, Eq. (43)] and rSCAN [red, Eq. (45)] DFAs.

using reference densities thought to be both accurate and close to the self-consistent density of the DFA; self-consistent tests are only performed after suitable parameters have been determined. Quite important for the present work, Ref. 48 also demonstrated that the optimal meta-GGA did not deviate dramatically from SCAN, possibly suggesting that SCAN is close to a fundamental limit on the accuracy of a meta-GGA. A recent fully nonlocal machine-learned functional[50,51] satisfies the constraints on fractional electron number[52] and fractional spin[53] by turning them into data that a machine can learn.

II. CONSTRAINT RESTORATION

A. Coordinate scaling and uniform density limit

The SCAN meta-GGA is comprised of distinct exchange and correlation functionals, each constructed as an interpolation and extrapolation of two semi-local energy densities: one for single-orbital densities $\epsilon^0_{x/c}$ and one for slowly varying densities $\epsilon^1_{x/c}$, where "x/c" is either exchange or correlation, respectively. Here, we will use ϵ to refer the energy density and $\varepsilon = \epsilon/n$ to refer the energy per electron. The single-orbital and slowly varying energy densities are joined by way of an interpolation function,

$$\epsilon^{\mathrm{SCAN}}_{x/c}(\boldsymbol{r}) = \epsilon^1_{x/c}(\boldsymbol{r}) + f_{x/c}(\alpha(\boldsymbol{r}))\left[\epsilon^0_{x/c}(\boldsymbol{r}) - \epsilon^1_{x/c}(\boldsymbol{r})\right], \tag{1}$$

which is controlled by the iso-orbital indicator variable,

$$\alpha = \frac{\tau - \tau_W}{\tau_U}. \tag{2}$$

α is built from three kinetic energy densities: the positive-definite conventional $\tau = 1/2\sum_i^{\mathrm{occ.}}|\nabla\phi_i|^2$ defined with the occupied Kohn–Sham orbitals $\{\phi_i\}$, von Weizsäcker $\tau_W = |\nabla n|^2/(8n)$ that is the single-orbital limit of τ as a function of the electron density $n = \sum_i^{\mathrm{occ.}}|\phi_i|^2$, and $\tau_U = \frac{3}{10}k_{\mathrm{F}}^2\, n\, d_s(\zeta)$, which is the uniform electron gas limit of τ, also called the Thomas–Fermi kinetic energy density or $\tau_{\mathrm{TF}}(n,\zeta)$. Here, the Fermi wavevector $k_{\mathrm{F}} = [3\pi^2 n]^{1/3}$ and $d_s(\zeta) = [(1+\zeta)^{5/3} + (1-\zeta)^{5/3}]/2$ is a function of the spin polarization $\zeta = (n_\uparrow - n_\downarrow)/(n_\uparrow + n_\downarrow)$. We refer to Refs. 5, 34, and 54–58 for a detailed discussion of the properties of α and related quantities.

The first change made in rSCAN[33] is to regularize the iso-orbital indicator to prevent divergence of the XC potential v_{xc} in the asymptotic regions of single-orbital systems.[34] This divergence is problematic for pseudo-potential generation.[33,34] In such regions, the derivative $\partial\alpha/\partial\tau$ diverges faster than the decay of $\epsilon_{\mathrm{x}}^{\mathrm{LDA}} = -3k_{\mathrm{F}}n/(4\pi)$ (the local density approximation for exchange), causing $|v_{\mathrm{xc}}| \to \infty$ when $\partial\epsilon_{\mathrm{xc}}/\partial\alpha \neq 0$,[34] as in SCAN. The regularized indicator α' used in rSCAN is

$$\tilde{\tau}_U = \left(\frac{3}{10}(3\pi^2)^{2/3}n^{5/3} + \tau_r\right)d_s(\zeta), \tag{3}$$

$$\tilde{\alpha} = \frac{\tau - \tau_W}{\tilde{\tau}_U}, \tag{4}$$

$$\alpha' = \frac{\tilde{\alpha}^3}{\tilde{\alpha}^2 + \alpha_r}. \tag{5}$$

The regularizing constants are $\tau_r = 10^{-4}$ and $\alpha_r = 10^{-3}$. While successful in preventing the rSCAN potential from diverging, the α' regularization breaks two exact constraints: (1) the uniform density limit and (2) the uniform coordinate scaling of the exchange energy.[59]

The exact uniform density limit is recovered in SCAN by recognizing

$$\lim_{|\nabla n|\to 0}\tau = \lim_{|\nabla n|\to 0}\tau_U \tag{6}$$

and

$$\lim_{|\nabla n|\to 0}\tau_W = 0. \tag{7}$$

Hence,

$$\lim_{|\nabla n|\to 0}\alpha = 1. \tag{8}$$

Then, by construction,

$$\lim_{|\nabla n|\to 0} f^{\mathrm{SCAN}}_{x/c}(\alpha) = 0, \tag{9}$$

and Eq. (1) exclusively selects ϵ_{x}^1 and ϵ_{c}^1 in the uniform density limit. These energy densities satisfy the uniform density limit by design.

The uniform density limit is broken by the regularization parameters in α' as

$$\lim_{|\nabla n|\to 0}\tilde{\tau}_U \neq \lim_{|\nabla n|\to 0}\tau, \tag{10}$$

$$\lim_{|\nabla n|\to 0}\tilde{\alpha} = \frac{\lim_{|\nabla n|\to 0}\tau_U}{\lim_{|\nabla n|\to 0}\tilde{\tau}_U} \neq 1, \tag{11}$$

$$\lim_{|\nabla n|\to 0}\alpha' \neq 1. \tag{12}$$

Hence,

$$\lim_{|\nabla n|\to 0} f^{\mathrm{rSCAN}}_{x/c}(\alpha') \neq 0. \tag{13}$$

The final inequality results in a slight scaling of $\epsilon_{x/c}^{1}$ and a small inclusion of $\epsilon_{x/c}^{0}$, which does not recover the uniform density limit. Hence, the constraint is broken. The uniform density limit is important for metallic elements. For a uniform electron gas of density parameter $r_s = 4$ (roughly characteristic of the valence electron density in solid sodium), $\alpha' \approx 0.719$, for example.

The regularized uniform electron gas kinetic energy density, $\tilde{\tau}_U$, also causes the exchange energy density to behave incorrectly under uniform coordinate scaling transformations. The density n and Kohn–Sham orbital ϕ_i scale as

$$n_\lambda(\boldsymbol{r}) = \lambda^3 n(\lambda \boldsymbol{r}), \tag{14}$$

$$\phi_{i,\lambda}(\boldsymbol{r}) = \lambda^{3/2}\phi_i(\lambda \boldsymbol{r}) \tag{15}$$

with $\lambda \geq 0$ such that the standard meta-GGA variables scale as

$$\tau_\lambda(\boldsymbol{r}) = \lambda^5 \frac{1}{2}\sum_i^{\text{occ.}} \left| \frac{\partial \phi_i(\lambda \boldsymbol{r})}{\partial(\lambda \boldsymbol{r})} \right|^2 = \lambda^5 \tau(\lambda \boldsymbol{r}), \tag{16}$$

$$\tau_{W,\lambda}(\boldsymbol{r}) = \lambda^5 \tau_W(\lambda \boldsymbol{r}), \tag{17}$$

$$\tau_{U,\lambda}(x,y,z) = \lambda^5 \tau_U(\lambda \boldsymbol{r}). \tag{18}$$

Thus, while $\alpha(\boldsymbol{r}) \to \alpha(\lambda \boldsymbol{r})$ under uniform coordinate scaling, $\tilde{\alpha}$ does not have this correct behavior except in the limit $\lambda \to \infty$ because the regularization τ_r in $\tilde{\tau}_U$ does not vary with the coordinate scaling parameter λ. This clearly violates the uniform coordinate scaling behavior of the exchange energy,[59]

$$E_x[n_\lambda] = \lambda E_x[n], \tag{19}$$

as $\tilde{\alpha}$ does not scale correctly, and the exchange and correlation models here are highly nonlinear in $\tilde{\alpha}$. The exact correlation energy evaluated on a uniformly scaled density tends to distinct limits,[60–62]

$$\lim_{\lambda\to\infty} E_c[n_\lambda] = \text{constant} \leq 0, \tag{20}$$

$$\lim_{\lambda\to 0} E_c[n_\lambda] = \lambda D_c[n], \tag{21}$$

where the finite constant and density functional D_c are unknown. It can be seen that SCAN and the DFAs presented here satisfy both limits, but rSCAN satisfies only the $\lambda \to \infty$ limit.

rSCAN does not violate known exact constraints[61,63,64] under nonuniform coordinate scaling. This is because the rSCAN exchange and correlation energies per electron inherit (from SCAN) boundedness under all one-dimensional non-uniform scalings. However, the rSCAN and SCAN meta-GGAs can have different limits under such non-uniform scalings, likely leading to different performance for some real systems. According to Eqs. (14) and (15), one-dimensional non-uniform scaling is

$$n_\lambda^x(x,y,z) = \lambda n(\lambda x, y, z), \tag{22}$$

$$\phi_{i,\lambda}^x(x,y,z) = \lambda^{1/2}\phi_i(\lambda x, y, z) \tag{23}$$

again with $\lambda \geq 0$. Under this coordinate transformation, the exact exchange energy satisfies[61,63]

$$\lim_{\lambda\to 0} \frac{1}{N} E_x[n_\lambda^x] > -\infty, \tag{24}$$

$$\lim_{\lambda\to\infty} \frac{1}{N} E_x[n_\lambda^x] > -\infty, \tag{25}$$

with N being the number of electrons. Similar inequalities hold for the exact correlation energy,[63,64]

$$\lim_{\lambda\to 0} \frac{1}{N} E_c[n_\lambda^x] = 0, \tag{26}$$

$$\lim_{\lambda\to\infty} \frac{1}{N} E_c[n_\lambda^x] > -\infty. \tag{27}$$

It should be emphasized that these constraints imply that the exact exchange and correlation energies per electron tend to finite constants under either limit of non-uniform coordinate scaling. The constant limits for Eqs. (25) and (27) are non-zero negative constants: the exchange and correlation energies per electron for a two-dimensional system.[64]

To recover these constraints on an approximate exchange energy functional, the exchange enhancement factor $F_x = \epsilon_x/\epsilon_x^{\text{LDA}}$ must satisfy[65,66]

$$\lim_{p\to\infty} F_x \propto p^{-1/4}. \tag{28}$$

$p = |\nabla n|^2/(2k_F n)^2 = s^2$ is the square of a dimensionless gradient of the density on the appropriate length scale for the exchange energy. We will discuss p further in the ensuing section on gradient expansions, but it suffices here to note that p scales as $\lambda^{-2/3}$ as $\lambda \to 0$ and as $\lambda^{4/3}$ as $\lambda \to \infty$, as shown in the supplementary material. Therefore, p is always divergent under the extreme limits of non-uniform coordinate scaling. In SCAN, rSCAN, and the DFAs developed here, the set of coordinate scaling constraints for exchange are imposed through a function $g_x(p)$,

$$F_x^{\text{SCAN}}(p,\alpha) = \{h_{1x}(p,\alpha) + f_x(\alpha)[h_{0x} - h_{1x}(p,\alpha)]\} g_x(p), \tag{29}$$

$$g_x(p) = 1 - \exp[-a_1 p^{-1/4}], \tag{30}$$

$$h_{0x} = 1 + \kappa_0 = 1.174, \tag{31}$$

$$h_{1x}(p,\alpha) = 1 + \kappa_1 - \frac{\kappa_1}{1 + \frac{x(p,\alpha)}{\kappa_1}}, \tag{32}$$

$$x(p,\alpha) = \mu p\left[1 + \left(\frac{b_4 p}{\mu}\right)\exp\left(\frac{-|b_4|p}{\mu}\right)\right] + \left\{b_1 p + b_2(1-\alpha)\exp\left[-b_3(1-\alpha)^2\right]\right\}^2. \tag{33}$$

Here, μ and b_i are constants that are determined by another constraint, the fourth order gradient expansion for exchange (GE4X),

discussed in Sec II B 1. Referring to Eq. (1), it can be seen that $h_{jx} = \epsilon_x^j/[\epsilon_x^{LDA} g_x(p)]$ with $j = 0, 1$. In the limit $p \to \infty$,

$$\lim_{p\to\infty} g_x(p) = a_1 p^{-1/4} + \mathcal{O}\left(p^{-1/2}\right), \tag{34}$$

$$\lim_{p\to\infty} h_{jx} = \text{constant} > 0, \quad j = 0, 1. \tag{35}$$

Thus, $F_x \sim p^{-1/4}$. In SCAN, rSCAN, and this work, $h_{0x} = 1.174$ identically, and $h_{1x}(p \to \infty) = 1 + \kappa_1 = 1.065$. These meta-GGAs produce finite exchange energies under non-uniform coordinate scaling, whereas the LDA, most GGAs, and many other meta-GGAs do not, as they do not recover the right asymptotic behavior of Eq. (28) for the exchange enhancement factor.

Recovering the analogous set of non-uniform coordinate scaling constraints for correlation is more straightforward and requires that the correlation energy per electron ε_c remains finite in two limits,

$$\lim_{r_s\to 0}\left[\lim_{p/r_s\to\infty} \varepsilon_c\right] = \text{constant} \le 0, \tag{36}$$

$$\lim_{r_s\to\infty}\left[\lim_{p/r_s\to\infty} \varepsilon_c\right] = 0, \tag{37}$$

where $r_s = [3/(4\pi n)]^{1/3}$ is the Wigner–Seitz radius. The order in which the limits are taken should not matter. In SCAN, rSCAN, and the DFAs developed here, both constants are chosen to be zero, although that choice incorrectly yields no correlation energy per electron in the true two-dimensional limit of a three-dimensional finite system. Many non-empirical GGAs and meta-GGAs for correlation satisfy the non-uniform coordinate scaling constraints. LDA, which has a logarithmic divergence as $r_s \to 0$, does not.

We can now consider the iso-orbital indicators used in SCAN, rSCAN, and r^{2}SCAN. Under the non-uniform coordinate scaling defined in Eqs. (22) and (23), the standard meta-GGA variables scale as

$$\tau_\lambda^x(x,y,z) = \frac{\lambda}{2}\sum_i^{\text{occ.}}\left|\hat{\boldsymbol{x}}\lambda\frac{\partial\phi_i(\lambda x,y,z)}{\partial(\lambda x)} + \nabla_\perp\phi_i(\lambda x,y,z)\right|^2, \tag{38}$$

$$\tau_{W,\lambda}^x(x,y,z) = \lambda\frac{\left|\hat{\boldsymbol{x}}\lambda\frac{\partial n(\lambda x,y,z)}{\partial(\lambda x)} + \nabla_\perp n(\lambda x,y,z)\right|^2}{8n(\lambda x,y,z)}, \tag{39}$$

$$\tau_{U,\lambda}^x(x,y,z) = \lambda^{5/3}\tau_U(\lambda x,y,z) \tag{40}$$

with

$$\nabla_\perp = \hat{\boldsymbol{y}}\frac{\partial}{\partial y} + \hat{\boldsymbol{z}}\frac{\partial}{\partial z}.$$

From these equations, we see that when $\lambda \to 0$, τ and τ_W scale as λ, but τ_U scales as $\lambda^{5/3}$. Thus, α scales with a leading order of $\lambda^{-2/3}$ in this limit. When $\lambda \to \infty$, α can either scale as $\lambda^{4/3}$ or $\lambda^{-2/3}$. Examples and analysis of both scaling limits are given in the supplementary material.

Due to the τ_r constant in the denominator of $\tilde{\alpha}$ [Eq. (4)], the leading-order behavior of the regularized $\tilde{\alpha}$ under non-uniform scaling, with $\lambda \to 0$ is λ. Then, whereas α tends to infinity in the $\lambda \to 0$ limit, $\tilde{\alpha}$ tends to zero. $\tilde{\alpha}$ has the correct leading-order behavior in the limit $\lambda \to \infty$, which can be a single-orbital limit where exact constraints, including the finite exchange and correlation energies under the nonuniform coordinate scaling, were built for SCAN.

In Ref. 37, we proposed an alternative regularization of α to restore these constraints,

$$\bar{\alpha} = \frac{\tau - \tau_W}{\tau_U + \eta\tau_W} = \frac{\alpha}{1 + \eta\frac{5}{3}p}, \tag{41}$$

where η is a regularization parameter to be determined later. Clearly, $\bar{\alpha}$ has the correct behavior, $\bar{\alpha}(\boldsymbol{r}) \to \bar{\alpha}(\lambda\boldsymbol{r})$ under uniform coordinate scaling. This regularization eliminates the asymptotic region ($|\boldsymbol{r}| \to \infty$) divergence and, by Eq. (7), does not change the uniform density limit,

$$\lim_{|\nabla n|\to 0}\bar{\alpha} = 1. \tag{42}$$

The nonuniform coordinate scaling of $\bar{\alpha}$ is also maintained as $\lambda^{-2/3}$ to leading order in the $\lambda \to 0$ limit. However, for $\lambda \to \infty$, the leading-order term of $\bar{\alpha}$ is independent of λ for non-homogeneous densities. This is demonstrated in the supplementary material.

Figure 1 shows a comparison of α, α', and $\bar{\alpha}$ for the krypton atom. The divergence of the conventional α is apparent in the asymptotic region, while α' and $\bar{\alpha}$ decay to 0. Close to the nucleus, the α_r regularization constant causes α' to behave differently to α and $\bar{\alpha}$, but otherwise, all three indicators behave similarly.

Substituting $\bar{\alpha}$ for α' in rSCAN is sufficient to restore the uniform density limit and coordinate scaling behaviors, and we refer to rSCAN with this replacement as "r++SCAN" throughout.

B. Gradient expansions

The interpolative design of SCAN allows for the construction of the single-orbital (ϵ^0) and slowly varying (ϵ^1) energy densities that consider only the exact constraints relevant to their respective limits. In SCAN, the interpolation function is a piece-wise combination of two exponential terms,

$$f_{x/c}(\alpha) = \begin{cases} \exp\left[\dfrac{-c_{1x/c}\alpha}{1-\alpha}\right], & \alpha \le 1, \\ -d_{x/c}\exp\left[\dfrac{c_{2x/c}}{1-\alpha}\right], & \alpha > 1, \end{cases} \tag{43}$$

where $\{d_{x/c}, c_{1x/c}, c_{2x/c}\}$ are separate parameters for exchange and correlation determined by fitting to appropriate norms.[5] This function was chosen such that (1) $f(\alpha = 0) = 1$ exclusively selects ϵ^0 for single-orbital densities, (2) $f(\alpha = 1) = 0$ exclusively selects ϵ^1 in slowly varying densities, and (3)

$$\left.\frac{df(\alpha)}{d\alpha}\right|_{\alpha\to 1} = \left.\frac{d^2 f(\alpha)}{d\alpha^2}\right|_{\alpha\to 1} = 0, \tag{44}$$

which prevents ϵ^0 contributing to the slowly varying density gradient expansions to the fourth order in $|\nabla n|$. Note $\left.\frac{d^m f(\alpha)}{d\alpha^m}\right|_{\alpha\to 1} = 0$ with m any non-negative integer in Eq. (43), by design. While theoretically convenient, Eq. (43) introduces a twist into the function

around $\alpha = 1$; see Fig. 2. This twist destroys the overall smoothness of the DFA, introduces oscillations into the XC potential,[33,34] and harms its performance on numerical integration grids.

The rSCAN meta-GGA uses a smooth polynomial interpolation function in place of the SCAN piece-wise exponential for the range $0 \le \alpha' < 2.5$,

$$f(\alpha') = \begin{cases} \sum_{i=0}^{7} c_i \alpha'^{\,i}, & 0 \le \alpha' \le 2.5, \\ -d_{x/c} \exp\left[\dfrac{c_{2x/c}}{1-\alpha'}\right], & \alpha' > 2.5, \end{cases} \tag{45}$$

where $\{c_i\}$ are polynomial coefficients determined to smoothly join $f^{\mathrm{SCAN}}(\alpha')$ at $\alpha' = 0$ and 2.5; see Ref. 33. A comparison of the two interpolation functions is shown in Fig. 2. While this replacement smooths the XC energy density and potential, it breaks the third constraint on the interpolation function, and hence, ϵ^0 makes spurious contributions to the slowly varying density gradient expansion of ϵ^1. Here, we restore the correct expansions by directly subtracting the extra terms that result from breaking the third condition [Eq. (44)] around $p \to 0$ and $\alpha \to 1$ where the expansion is relevant.

The exact gradient expansion for exchange around the slowly varying density limit to the second order (GE2X) and to the fourth order (GE4X) was derived in terms of the exchange enhancement factor F_x in Refs. 69–72 as

$$\lim_{|\nabla n|\to 0} F_x^{\mathrm{GE}} = 1 + \mu p + \frac{146}{2025}\tilde{q}^2 - \frac{73}{405} p\tilde{q} + \mathcal{O}\left[|\nabla n|^6\right], \tag{46}$$

where $\mu = 10/81$ and $\tilde{q} = (9/20)(\tilde{\alpha} - 1) + (3\eta/4 + 2/3)p$ recovers the reduced density Laplacian, $q = \nabla^2 n/(4k_F^2 n)$, as $|\nabla n| \to 0$. The gradient expansion for correlation was derived to the second order (GE2C) in Refs. 5, 42, 73, and 74 as

$$\varepsilon_c = \varepsilon_c^{\mathrm{LSDA}} + \beta(r_s)\phi(\zeta)^3 t(r_s,\zeta,p)^2 + \mathcal{O}\left[|\nabla n|^4\right], \tag{47}$$

where $\phi(\zeta) = \left[(1+\zeta)^{2/3} + (1-\zeta)^{2/3}\right]/2$ and $t(r_s,\zeta,p) = (3\pi^2/16)^{1/3}\sqrt{p/r_s}/\phi(\zeta)$. Next, we restore each of these expansions to r++SCAN in turn.

1. Exchange

The SCAN exchange enhancement factor for a spin-unpolarized system is given in Eqs. (29)–(33). The constants $\mu = 10/81$ and $\{b_1, b_2, b_3, b_4\}$ appearing in Eq. (33) are chosen such that SCAN yields GE2X and GE4X, noting that the expansion of $g_x(p)$ around $p = 0$ has only zero-order contributions (see the supplementary material).

In rSCAN, the interpolation function derivatives are non-zero at $\tilde{\alpha} = 1$, so h_{0x} also contributes to the gradient expansion. This changes the DFA's gradient expansion, spoiling the correct gradient expansion of the $x(p,\alpha)$ inherited from SCAN. Thus, both rSCAN and r++SCAN fail to recover GE2X and GE4X.

We restore GE2X to give the r^{2}SCAN exchange functional by redesigning $x(p,\alpha)$ as

$$x(p) = \left(C_\eta C_{2x} \exp\left[-p^2/d_{p2}^4\right] + \mu\right)p, \tag{48}$$

where C_η and C_{2x} are constants set to cancel spurious contributions from h_{0x} to the second order in ∇n. The restoring constants are multiplied by the damping function $\exp[-p^2/d_{p2}^4]$ to prevent them dominating as p becomes large. The damping parameter d_{p2} derives from scaling the reduced density gradient as $s \to s/d_{p2}$ with d_{p2} fit to recover the appropriate norms in Sec. IV.

To find C_η and C_{2x}, we take the Taylor expansion of the rSCAN interpolation function [Eq. (45)] around $\tilde{\alpha} = 1$, noting that $1 - \tilde{\alpha}$ is $\mathcal{O}\left[|\nabla n|^2\right]$,

$$\lim_{|\nabla n|\to 0} f^{\mathrm{rSCAN}}(\tilde{\alpha}) = -(1-\tilde{\alpha})\Delta f_2 + \frac{(1-\tilde{\alpha})^2}{2}\Delta f_4 + \mathcal{O}\left[|\nabla n|^6\right], \tag{49}$$

where

$$\Delta f_2 = \sum_{i=1}^{7} i c_i, \tag{50}$$

$$\Delta f_4 = \sum_{i=2}^{7} i(i-1)c_i \tag{51}$$

are determined by the first and second derivatives of the interpolation function with respect to $\tilde{\alpha}$, respectively.

The $(1-\tilde{\alpha})$ term of Eq. (49) indicates a fixed slope for the $\tilde{\alpha}$ dependence of the enhancement factor across the slowly varying limit that is found to be numerically problematic, further analyzed in Sec. III. This can be avoided to second order by expressing $(1-\tilde{\alpha})$ in terms of p through an integration by parts on the exchange energy density,[75]

$$\lim_{|\nabla n|\to 0}(1-\tilde{\alpha}) = \left(\frac{20}{27} + \eta\frac{5}{3}\right)p + \mathcal{O}\left[|\nabla n|^4\right]. \tag{52}$$

This substitution, derived and discussed in the supplementary material, is used in r^{2}SCAN and identifies

$$C_\eta = (20/27 + \eta 5/3). \tag{53}$$

To second order, the slowly varying gradient expansion of r^{2}SCAN is given by

$$\lim_{|\nabla n|\to 0} F_x^{\mathrm{r^2SCAN}} = \lim_{|\nabla n|\to 0} h_{1x} - C_\eta p \Delta f_2 \left(h_{0x} - \lim_{|\nabla n|\to 0} h_{1x}\right). \tag{54}$$

Finding

$$\lim_{|\nabla n|\to 0} h_{1x} = 1 + (\mu + C_\eta C_{2x})p + \mathcal{O}\left[|\nabla n|^4\right] \tag{55}$$

and collecting terms give

$$\lim_{|\nabla n|\to 0} F_x^{\mathrm{r^2SCAN}} = 1 + \mu p + C_\eta[C_{2x} - \Delta f_2 h_{0x} + \Delta f_2]p + \mathcal{O}\left[|\nabla n|^4\right]. \tag{56}$$

Equating this to GE2X [second order and below terms of Eq. (46)] and solving for C_{2x} give

$$C_{2x} = -\Delta f_2(1 - h_{0x}) \approx -0.162\,742, \tag{57}$$

as shown in the supplementary material.

GE4X can be restored to give the "r^{4}SCAN" meta-GGA by including a further correcting term in the exchange enhancement

factor outside the interpolation. This introduces three more constants, derived in the supplementary material, for all terms in Eq. (46),

$$F_x^{r^4SCAN}(p,\tilde{\alpha}) = \{h_{1x}(p) + f_x(\tilde{\alpha})[h_{0x} - h_{1x}(p)] + \Delta F_4(p,\tilde{\alpha})\}g_x(p), \tag{58}$$

$$\Delta F_4(p,\tilde{\alpha}) = \{C_{2x}[(1-\tilde{\alpha}) - C_\eta p] + C_{\tilde{\alpha}\tilde{\alpha}}(1-\tilde{\alpha})^2 + C_{p\tilde{\alpha}}p(1-\tilde{\alpha}) + C_{pp}p^2\}\Delta F_4^{\text{damp}}(p,\tilde{\alpha}), \tag{59}$$

$$\Delta F_4^{\text{damp}}(p,\tilde{\alpha}) = \frac{2\tilde{\alpha}^2}{1+\tilde{\alpha}^4}\exp\left[-\frac{(1-\tilde{\alpha})^2}{d_{\tilde{\alpha}4}^2} - \frac{p^2}{d_{p4}^4}\right], \tag{60}$$

$$C_{\tilde{\alpha}\tilde{\alpha}} = \frac{73}{5000} - \frac{\Delta f_4}{2}[h_{0x} - 1] \approx -0.059\,353\,1, \tag{61}$$

$$C_{p\tilde{\alpha}} = \frac{511}{13\,500} - \frac{73}{1500}\eta - \Delta f_2[C_\eta C_{2x} + \mu] \approx 0.040\,268\,4, \tag{62}$$

$$C_{pp} = \frac{146}{2025}\left\{\eta\frac{3}{4} + \frac{2}{3}\right\}^2 - \frac{73}{405}\left\{\eta\frac{3}{4} + \frac{2}{3}\right\} + \frac{(C_\eta C_{2x} + \mu)^2}{k_1} \approx -0.088\,076\,9. \tag{63}$$

Further damping functions, ΔF_4^{damp}, are included to prevent the correction terms dominating as $(1-\tilde{\alpha})$ and p become large, introducing $d_{\tilde{\alpha}4}$ and d_{p4} as additional parameters. These are again set to recover the appropriate norms in Sec. IV. For the fourth order expansion, the integration by parts substitution of Eq. (52) cannot be applied, and hence, $(1-\tilde{\alpha})$ cannot be removed.

2. Correlation

The SCAN model of the correlation energy per electron $\varepsilon_c = \epsilon_c/n$ is

$$\varepsilon_c^{\text{SCAN}} = \varepsilon_c^1 + f_c^{\text{SCAN}}(\alpha)\left[\varepsilon_c^0 - \varepsilon_c^1\right], \tag{64}$$

with the $\alpha = 0$ correlation energy per electron given by

$$\varepsilon_c^0 = \left(\varepsilon_c^{\text{LDA0}} + H_c^0\right)g_c(\zeta), \tag{65}$$

$$\varepsilon_c^{\text{LDA0}} = -\frac{b_{1c}}{1 + b_{2c}\sqrt{r_s} + b_{3c}r_s}, \tag{66}$$

$$H_c^0 = b_{1c}\ln\{1 + w_0[1 - g_\infty(p)]\}, \tag{67}$$

$$w_0 = \exp\left[-\varepsilon_c^{\text{LDA0}}/b_{1c}\right] - 1, \tag{68}$$

$$g_\infty(p) = (1 + 4\chi_\infty p)^{-1/4}, \tag{69}$$

$$g_c(\zeta) = \{1 - 2.3631[d_x(\zeta) - 1]\}\left(1 - \zeta^{12}\right) \tag{70}$$

with $d_x(\zeta) = [(1+\zeta)^{4/3} + (1-\zeta)^{4/3}]/2$.

Similarly, the $\alpha = 1$ limit is given by

$$\varepsilon_c^1 = \varepsilon_c^{\text{LSDA}} + H_c^1, \tag{71}$$

$$H_c^1 = \gamma\phi^3\ln\{1 + w_1[1 - g(y)]\}, \tag{72}$$

$$w_1 = \exp\left[-\frac{\varepsilon_c^{\text{LSDA}}}{\gamma\phi^3}\right] - 1, \tag{73}$$

$$g(y) = (1+4y)^{-1/4}, \tag{74}$$

$$y = \frac{\beta(r_s)}{\gamma w_1}t^2, \tag{75}$$

$$\beta(r_s) = \beta_{\text{MB}}\frac{1 + Ar_s}{1 + Br_s}, \tag{76}$$

where $b_{1c} = 0.028\,576\,4$, $b_{2c} = 0.0889$, $b_{3c} = 0.125\,541$, $\chi_\infty = 0.128\,026$, $\gamma = 0.031\,090\,7$, $\beta_{\text{MB}} = 0.066\,725$, $A = 0.1$, and $B = 0.1778$. $\varepsilon_c^{\text{LSDA}}$ is the local spin-density approximation for correlation from Ref. 76.

As r++SCAN takes the same correlation model, the violation of Eq. (44) by the rSCAN interpolation function breaks GE2C. The GE2C correction terms are restored to r++SCAN by replacing $g(y)$ in ϵ_c^1 with

$$g(y,\Delta y) = [1 + 4(y - \Delta y)]^{-1/4}, \tag{77}$$

$$\Delta y = \frac{\Delta f_{c2}}{27\gamma d_s(\zeta)\phi^3 w_1}\left\{20r_s\left[g_c(\zeta)\frac{\partial\varepsilon_c^{\text{LDA0}}}{\partial r_s} - \frac{\partial\varepsilon_c^{\text{LSDA}}}{\partial r_s}\right] - 45\eta\left[\varepsilon_c^{\text{LDA0}}g_c(\zeta) - \varepsilon_c^{\text{LSDA}}\right]\right\}p\exp\left[-p^2/d_{p2}^4\right], \tag{78}$$

where the damping function $\exp[-p^2/d_{p2}^4]$ is the same as in Eq. (48). Similarly to exchange, we restore the second order slowly varying density gradient expansion when

$$\Delta f_{c2} \approx -0.711\,402. \tag{79}$$

The derivation of this expression is shown in the supplementary material.

Making these replacements to r++SCAN gives the "r^{2}SCAN" meta-GGA, which only breaks GE4X. Including the full correction of Eq. (58) gives the "r^{4}SCAN" meta-GGA, which obeys all the exact constraints SCAN does. For convenience, a collected definition of the working equations for all new DFAs is given in the supplementary material.

3. Summary of changes

Here, we summarize the changes made from SCAN for each of the DFAs.

1. rSCAN replaces α with α' of Eq. (5), which contains two regularization parameters $\tau_r = 10^{-4}$ and $\alpha_r = 10^{-3}$. It also replaces the SCAN interpolation function with a polynomial between $0 \le \alpha' \le 2.5$.
2. r++SCAN evolves from rSCAN, by replacing α' with $\bar{\alpha}$, of Eq. (41), which uses only a single regularization parameter, $\eta = 0.001$.
3. r^{2}SCAN inherits all the changes of r++SCAN. Additionally, for exchange, it replaces $x(p,\alpha)$ in h_{1x} with Eq. (48). For correlation, it replaces $g(y)$ with Eqs. (77) and (78) in ϵ_c^1.
4. r^{4}SCAN inherits all the changes from r^{2}SCAN. Additionally, for exchange, it replaces F_x with Eq. (58), which introduces ΔF_4 of Eq. (59).

III. NUMERICAL CHALLENGES

The corrections to restore the slowly varying density gradient expansions for exchange and correlation contain terms linear in $(1-\bar{\alpha})$. These terms are necessary to restore the second or fourth order gradient expansion, for example, of Eq. (46) for exchange if the integration by parts is not used as we did for r^{2}SCAN in Eq. (52). These corrections inevitably twist the slope of the interpolation function $f(\bar{\alpha})$ to that of F_x^{GE} with respect to $\bar{\alpha}$ around $\bar{\alpha} \to 1$ as $|\nabla n| \to 0$, illustrated in Fig. 3. This introduces oscillations into the derivatives of the enhancement factor with respect to $\bar{\alpha}$ and, hence, into the overall exchange–correlation potential. Such oscillations are undesirable and reintroduce the numerical problems rSCAN regularizes away. As the gradient expansion constraint requires

$$\left.\frac{\partial F_x}{\partial \bar{\alpha}}\right|_{\bar{\alpha}=1,p=0} \propto \left.\frac{df(\bar{\alpha})}{d\bar{\alpha}}\right|_{\bar{\alpha}=1}, \tag{80}$$

this oscillation in derivatives must be present, at least in the interpolation scheme discussed here, and cannot be removed by damping. Figure 3 compares uncorrected exchange enhancement, $d_{\bar{\alpha}4} \to 0$, the exchange enhancement with no damping on the correction terms, $d_{\bar{\alpha}4} \to \infty$, and $d_{\bar{\alpha}4} = 0.178$, determined in Sec. IV, showing this effect.

These numerical problems are not present in r^{2}SCAN as the corrections do not depend on $(1-\bar{\alpha})$. Thus, the corresponding oscillation in derivative is avoided, allowing r^{2}SCAN to recover GE2X and GE2C while maintaining a smooth potential. As the integration by parts is not possible to fourth order, r^{4}SCAN necessarily suffers an oscillatory XC potential in order to recover GE4X.

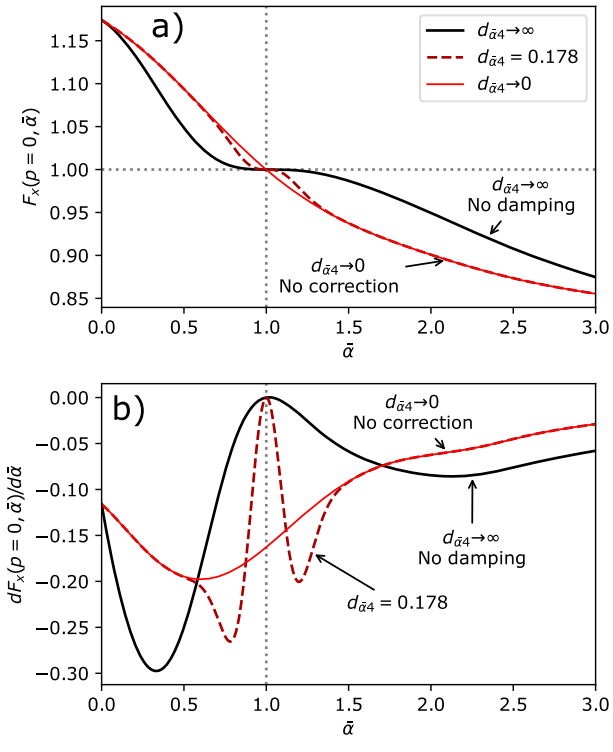

FIG. 3. (a) Exchange enhancement factor for r^{4}SCAN as a function of $\bar{\alpha}$ at $p = 0$. The uncorrected enhancement with $d_{\bar{\alpha}4} \to 0$ (red) is contrasted against the undamped corrections with $d_{\bar{\alpha}4} \to \infty$ (black lines), the proposed r^{4}SCAN damping of $d_{\bar{\alpha}4} = 0.178$ (dark red dashed lines). (b) Derivative of the exchange enhancement with respect to $\bar{\alpha}$ at $p = 0$ for the same conditions.

IV. DETERMINING PARAMETERS

The regularization of the $\bar{\alpha}$ indicator in r++SCAN, r^{2}SCAN, and r^{4}SCAN is controlled by the parameter η, with larger values increasing regularization strength. We find that performance is largely insensitive to η within the range of $0 \le \eta \le 0.001$ and take the upper value of $\eta = 0.001$.

We introduce a single damping parameter, d_{p2}, in r^{2}SCAN through Eqs. (48) and (78) and set it using the appropriate norm philosophy of the SCAN DFA. The parameter was chosen to minimize the sum of the mean absolute percentage errors in XC energy for four rare gas atoms: Ne, Ar, Kr, and Xe (evaluated for spherical Hartree–Fock orbitals[67] relative to reference energies from Refs. 77–79), and four jellium surface formation energies with $r_s = 2$, 3, 4, and 6 bohrs (relative to reference energies from Ref. 80). As the parameters are not fit to any bound systems, we regard the resulting DFAs as non-empirical.

Objective error as a function of damping parameter, d_{p2}, is shown in Fig. 4. Setting the damping parameter too high degrades accuracy for the rare gas atoms (while mildly improving the jellium surface formation energies) as the gradient expansion terms dominate too far from $|\nabla n| \to 0$. Conversely, setting d_{p2} too small degrades accuracy for the jellium surfaces, as the second order gradient expansion is not sufficiently corrected. As a sharper damping function causes sharper features in XC potential, we take the largest value for d_{p2}, which meets the accuracy threshold defined by SCAN: a mean absolute percentage error (MAPE) of 0.1% for rare gas atom XC energies and 5% for jellium surfaces. The optimizing value is found as $d_{p2} = 0.361$.

Two additional parameters are introduced in r^{4}SCAN that controls damping of the fourth order gradient expansion terms. These were determined similarly as those which minimize a normalized sum of the rare gas atom and jellium surface mean absolute

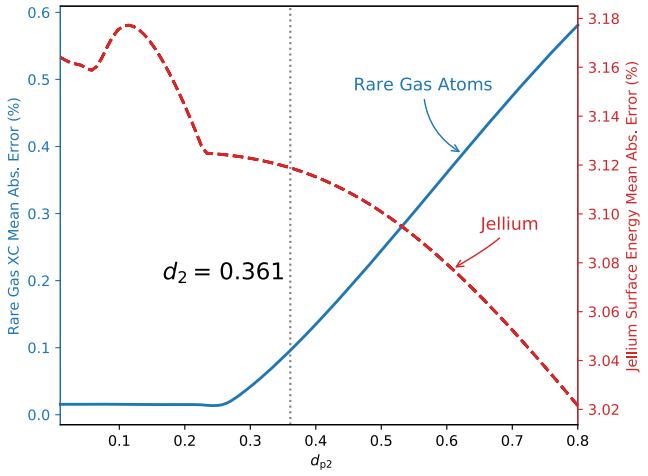

FIG. 4. The mean absolute percentage error for (left axis, blue) the exchange–correlation energies of Ne, Ar, Kr, and Xe[77–79] and (right axis, red) the exchange–correlation jellium surface energy for $r_s = \{2, 3, 4, 6\}$[80] as a function of second order gradient expansion damping parameter d_{p2} for r^{2}SCAN. The optimal value is chosen as the largest for which the rare gas atom error is <0.1%, and the jellium error is <5%.

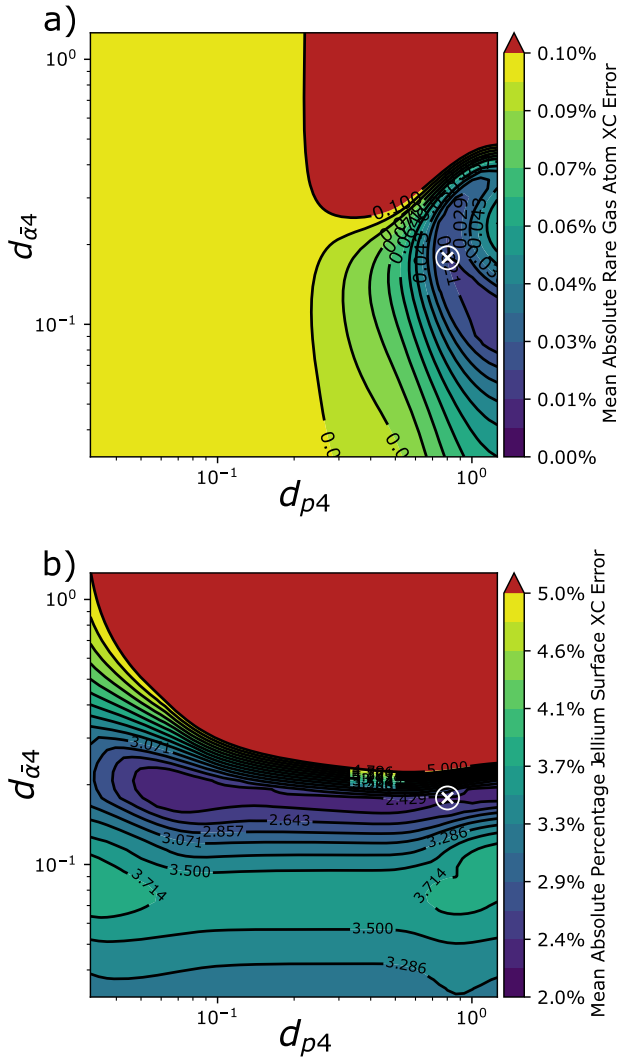

FIG. 5. Mean absolute percentage error in (a) rare gas atom XC energy and (b) jellium surface exchange–correlation energy as a function of damping parameters $d_{\bar{\alpha}4}$ and d_{p4}. Optimal parameters are identified by the white circled cross at $d_{p4} = 0.802$, $d_{\bar{\alpha}4} = 0.178$.

percentage errors. The minimizing parameters were found as $d_{\bar{\alpha}4} = 0.178$ and $d_{p4} = 0.802$, as shown in Fig. 5.

V. RESULTS

A. Enhancement factors and derivatives

An important principle in DFA design is to take an "Occam's razor" approach and determine a DFA that is free of twists and kinks. In this way, the DFA avoids over-fitting to data and ensures smooth functional derivatives that are easy to render on numerical grids.

Figure 6 compares the XC enhancement factors of SCAN, r^{2}SCAN, and r^{4}SCAN for the xenon atom. The SCAN enhancement factor shows sharp plateau-like regions from the twists in its interpolation function around $\alpha = 1$. The smooth polynomial interpolation function removes these plateaus in r^{2}SCAN, although some twists are re-introduced in r^{4}SCAN by the $(1 - \bar{\alpha})$ terms in the GE4X restoration.

The effect of twists in F_{xc} can be seen in the semi-local and non-local XC potential components of the XC potential, shown in Fig. 6. The SCAN meta-GGA shows sharp oscillations and drops in its non-local component around $\alpha = 1$. In contrast, the r^{2}SCAN meta-GGA is a smooth function of its ingredients and, hence, has smooth semi-local and non-local components in its XC potential. While the potential components of r^{2}SCAN and r^{4}SCAN coincide for much of space, they differ significantly around $\bar{\alpha} = 1$ points. Here, the $(1 - \bar{\alpha})$ correction terms in r^{4}SCAN required for GE4X cause sharp oscillations that return the problematic behavior we aim to remove. As these terms cannot be removed by partial integration to the fourth order in ∇n, we, therefore, conclude that GE4X is incompatible with functional smoothness under the present SCAN interpolation-based model: one must either twist the interpolation function to enforce Eq. (44) or include correcting terms that re-introduce oscillatory factors.

B. Appropriate norms

Appropriate norms are defined in Ref. 5 as "systems for which semilocal DFAs can be exact or extremely accurate." Here, like SCAN, we take these as the exchange and correlation energies of four rare gas atoms (Ne, Ar, Kr, and Xe), the exchange and correlation surface energies of four jellium slabs ($\overline{r_s} = 2$, 3, 4, and 6), and the interaction energy of Ar_2 at repulsive inter-atomic distances ($R_{Ar-Ar} = 1.6$, 1.8, and 2.0 Å). Table I compares the accuracy of SCAN, rSCAN, r++SCAN, r^{2}SCAN, and r^{4}SCAN for the appropriate norms.

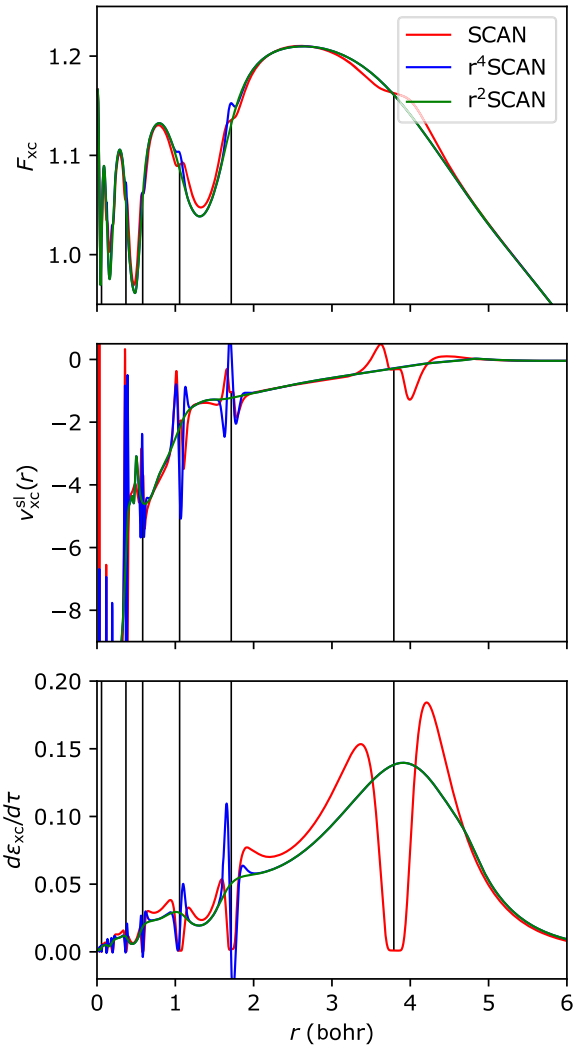

FIG. 6. The XC enhancement factor (top), the multiplicative component of the XC potential (middle), and the non-local component, i.e., the derivative of the XC energy density with respect to the orbital dependent kinetic energy density, τ (bottom) in the Xe atom, shown for the SCAN, r^{2}SCAN, and r^{4}SCAN meta-GGAs, calculated from reference Hartree–Fock datasets with Slater-type orbitals.[67,68] Points where $\alpha = 1$ are shown by black vertical lines.

Care must be taken when computing the jellium surface energy for rSCAN as the uniform bulk density energy is changed by the α' regularization. To evaluate the exchange–correlation contribution to the jellium surface formation energy, we compute[81]

$$\sigma_{xc}(\overline{r_s}) = \int_{-\infty}^{\infty} [\varepsilon_{xc}(n, \nabla n, \tau) - \varepsilon_{xc}(\overline{n}, 0, \overline{\tau_U})] n(x) dx, \qquad (81)$$

where $\overline{r_s} = (4\pi\overline{n}/3)^{-1/3}$ is the density parameter of the corresponding bulk jellium and $\overline{\tau_U} = 3(3\pi^2)^{2/3}\overline{n}^{5/3}/10$ is its kinetic energy density. Here, we have assumed that the surface lies along the x direction. This ensures that the uniform density limit of a given DFA is used, regardless of whether that uniform limit is the LSDA. Building upon our previous example of the valence density in solid sodium, when $r_s = 4$, the rSCAN exchange uniform density limit is

$$\epsilon_x^{rSCAN}(\overline{n}, 0, \overline{\tau_U})\big|_{\overline{r_s}=4} \approx 1.051 \epsilon_x^{LDA}(\overline{r_s}),$$

making a substantial error over LDA exchange. For $\overline{r_s} = 6$, this error is increased to roughly 14%.

The importance of recovering the second order gradient expansion is seen in the relative accuracy of the DFAs for the rare gas atoms. The two DFAs that do not recover the gradient expansions (rSCAN and r++SCAN) have MAPEs of ≈0.25%, whereas the DFAs that do have MAPEs of ≈0.1%. Restoring the fourth order gradient expansion for exchange improves accuracy further, although r^{2}SCAN already has similar accuracy to SCAN for all the appropriate norms, suggesting that GEX4 is less important for these systems. Outside of these differences, all DFAs performed similarly for the appropriate norm systems.

C. Atomization energies

The work of Ref. 35 shows that the performance of rSCAN is relatively poor for atomization energy prediction, as measured by its increased error for the G3 test set of molecules.[83] Table II compares the errors for this test set for all the DFAs derived above. Consistent with Ref. 35, we find a large error from rSCAN, with this error only slightly corrected in r++SCAN. As in Ref. 37, restoration of GE2X and GE2C in r^{2}SCAN restores the good accuracy of SCAN, showing the importance of these constraints for atomization energies. The good accuracy of r^{2}SCAN suggests that recovering GE4X is not essential for accurately predicting atomization energies.

The improved numerical performance of the DFAs is illustrated by examining the convergence of atomization energy predictions as a function of numerical grid density, as shown in Fig. 7. The original SCAN meta-GGA shows wild variation with changing grid density, with a range of over 6 kcal/mol in mean absolute error. While there is some indication that a convergence is approached for the most dense grids, the results from more computationally efficient grids are problematic and clearly untrustworthy.

All four regularized DFAs show very fast grid convergence, with all sparse grids giving close agreement to the dense grids. Given the sharp oscillations in Fig. 6 and analysis of Sec. III, it is somewhat unexpected that r^{4}SCAN shows good convergence with grid density. We attribute the improved performance over SCAN to the reduction in plateau-like behavior of F_{xc} but caution that grid convergence behavior will likely be more system dependent for r^{4}SCAN than r++SCAN and r^{2}SCAN as a result of the oscillations.

It is similarly unexpected to find that the accuracy of r^{2}SCAN is degraded by the inclusion of the GE4X in r^{4}SCAN. This supports our previous conclusion that GE4X is not important for

TABLE II. Summary of atomization energy errors (in kcal/mol) for the G3 test set[83] using the most dense numerical integration grid (TURBOMOLE level 7).

	SCAN	rSCAN	r++SCAN	r^{2}SCAN	r^{4}SCAN
ME	−5.036	−14.010	−12.912	−5.042	−6.939
MAE	6.121	14.258	13.239	5.866	7.716

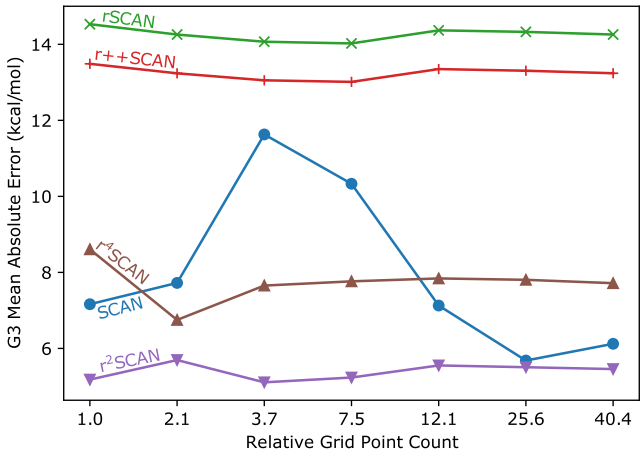

FIG. 7. Mean absolute percentage error of atomization energies (kcal/mol) for the G3 set of 226 molecules[83] as a function of increasing numerical integration grid density expressed relative to the smallest grid. The grids chosen were defined by the default TURBOMOLE grid levels. The mean number of grid points per atom over the G3 set is about 1326 for the smallest (gridsize = 1) and 53 590 for the largest (gridsize = 7) grid shown here.

the properties tested here and elsewhere.[40,41] We take the mild degradation of G3 accuracy from extending to r^{4}SCAN as further evidence that this method of including GE4X into interpolation-based meta-GGA DFAs is problematic. The inclusion of two additional fitting parameters beyond those in r^{2}SCAN may also contribute.

D. Further testing

Beyond atomization energies, we have tested the accuracy of the progression of SCAN-like DFAs for the interaction energies of closed shell complexes (S22)[84] and reaction barrier heights (BH76),[85] summarized in Table III. Additionally, Table IV summarizes accuracy for the LC20 set of lattice constants for solids,[86] obtained by fitting the stabilized jellium equation of state[87] to single point energy calculations at a range of lattice volumes. The individual bulk moduli of the LC20 solids are presented in Table S10 of the supplementary material; error statistics are given in Table V. All five DFAs gave comparable good accuracy across all three test sets, showing that SCAN's good performance is not significantly changed by the regularizations or exact constraint restoration for these properties.

TABLE III. Mean error (ME) and mean absolute error (MAE), both in kcal/mol, of SCAN,[5] rSCAN,[33] r++SCAN, r^{2}SCAN,[37] and r^{4}SCAN for the S22 set of 22 interaction energies between closed shell complexes[84] and the BH76 set of 76 chemical barrier heights.[85] Full data are presented in Tables S6 and S7 of the supplementary material. All calculations use the most dense integration grid (TURBOMOLE level 7).

		SCAN	rSCAN	r++SCAN	r^{2}SCAN	r^{4}SCAN
S22	ME	−0.524	−1.153	−0.554	−0.937	−0.874
	MAE	0.786	1.273	0.846	1.057	1.015
BH76	ME	−7.653	−7.365	−7.488	−7.125	−7.463
	MAE	7.724	7.434	7.556	7.182	7.527

TABLE IV. Error in lattice constant prediction for the LC20 lattice constant test set.[86] Errors ($a_0^{approx} - a_0^{expt.}$) are in Å relative to zero-point anharmonic expansion corrected experimental data from Ref. 88. Lattice constants were obtained by fitting the stabilized jellium equation of state[87] to single point energy calculations at a range of lattice volumes.

	Expt.	SCAN	rSCAN	r++SCAN	r^{2}SCAN	r^{4}SCAN
Ag	4.063	0.012	0.028	0.026	0.034	0.017
Al	4.019	−0.012	−0.027	−0.031	−0.032	−0.014
Ba	5.004	0.049	0.100	0.046	0.076	0.062
C	3.555	−0.004	−0.001	−0.001	0.005	0.002
Ca	5.555	−0.009	0.017	−0.011	0.018	0.016
Cu	3.595	−0.030	−0.023	−0.025	−0.020	−0.027
GaAs	5.641	0.020	0.031	0.026	0.029	0.017
Ge	5.644	0.029	0.043	0.038	0.039	0.028
Li	3.451	0.011	0.021	0.006	0.016	0.010
LiCl	5.072	0.016	0.021	0.017	0.034	0.032
LiF	3.974	0.004	0.008	0.008	0.021	0.020
MgO	4.188	0.018	0.019	0.018	0.027	0.024
NaCl	5.565	0.010	0.025	0.015	0.036	0.036
NaF	4.570	0.006	0.015	0.012	0.028	0.028
Na	4.207	−0.007	0.024	−0.012	0.004	0.031
Pd	3.876	0.016	0.026	0.026	0.032	0.019
Rh	3.793	−0.005	0.006	0.005	0.008	−0.005
Si	5.422	0.005	0.012	0.009	0.018	0.016
SiC	4.348	0.002	−0.001	−0.002	0.006	0.007
Sr	6.042	0.039	0.064	0.019	0.056	0.095
ME		0.009	0.020	0.009	0.022	0.021
MAE		0.015	0.026	0.018	0.027	0.025

TABLE V. Error statistics (in GPa) for the bulk moduli of the solids in the LC20 set.[86] Reference experimental values[89] include zero-point energy corrections. For the individual bulk modulus data, see Table S10 of the supplementary material.

	SCAN	rSCAN	r++SCAN	r^{2}SCAN	r^{4}SCAN
ME	3.424	1.879	2.667	1.483	2.216
MAE	6.316	5.749	5.984	5.887	5.916

VI. CONCLUSIONS

To summarize, we have shown how exact constraints obeyed by SCAN are broken by the regularizations in rSCAN. Through this analysis, we have shown how exact constraint adherence can be restored and how this can be achieved without sacrificing the good numerical performance of rSCAN. This results in three new DFAs with increasing exact constraint adherence: r++SCAN, r^{2}SCAN, and r^{4}SCAN. Additional parameters introduced to the new DFAs are set without reference to any real bonded systems; thus, we can still regard the resulting DFAs as non-empirical and expect them to

be applicable to a wide range of systems. Figure 7 suggests that restoring GEX4 in r^{4}SCAN gives similar accuracy to SCAN with some improvement in grid efficiency. We, therefore, expect the new r^{2}SCAN meta-GGA to remain the preferred choice for situations where the accuracy of SCAN is desired, but its use is prohibited by poor numerical performance.[31,90]

Further improvement over r^{2}SCAN might be achieved by a smoother and fuller incorporation of the fourth order density gradient terms for the exchange energy in a SCAN-like DFA. Work on this is under way.

Figure 7 shows that rSCAN and r++SCAN, which lose the correct second order gradient expansions for densities that vary slowly over space, also lose accuracy for atomization energies of molecules and that the restoration of this limit in SCAN, r^{2}SCAN, and r^{4}SCAN also restores accurate atomization energies. This result is in line with arguments made in Ref. 91.

Experience with SCAN and r^{2}SCAN (and with atomic densities[92]) suggests that smoothness at a fixed electron number could be elevated to the status of an 18th exact constraint that a meta-GGA can satisfy or at least to the status of a construction principle: By Occam's razor, the simplest assumption, consistent with what is known, should be preferred.

SUPPLEMENTARY MATERIAL

See the supplementary material for the following: additional derivations and data to complement those presented in the main text; a derivation of the r^{2}SCAN and r^{4}SCAN meta-GGAs presented in Appendix A; a further discussion of nonuniform coordinate scaling presented in Appendix B; all equations and constants needed to perform calculations with r^{2}SCAN and r^{4}SCAN shown in Appendix C, with reference calculations presented in Appendix D; the exchange–correlation potential in the Xe atom presented in Appendix E; data for the test sets considered here for SCAN, rSCAN, r++SCAN, r^{2}SCAN, and r^{4}SCAN presented in Appendixes F–H; the G3 set in Appendix F; the S22 and BH76 sets in Appendix G; and the LC20 set in Appendix H.

ACKNOWLEDGMENTS

J.W.F., J.N., and J.S. acknowledge the support from the U.S. DOE, Office of Science, Basic Energy Sciences, under Grant No. DE-SC0019350. J.S. also acknowledges the support from the U.S. National Science Foundation under Grant No. DMR-2042618. A.D.K. acknowledges the support from the U.S. Department of Energy, Office of Science, Basic Energy Sciences, through Grant No. DE-SC0012575 to the Energy Frontier Research Center: Center for Complex Materials from First Principles and also the support from Temple University. J.P.P. acknowledges the support from the U.S. National Science Foundation under Grant No. DMR-1939528. The authors would like to thank Albert Bartók-Partay and Daniel Mejía-Rodríguez for their invaluable discussions around the ideas presented here. J.P.P. and J.S. thank Natalie Holzwarth for pointing out that the SCAN exchange–correlation potential for an atom diverges in the tail of the density, making pseudo-potential construction difficult.

AUTHOR DECLARATIONS

Conflict of Interest

The authors have no conflicts to disclose.

DATA AVAILABILITY

r^{2}SCAN and r^{4}SCAN subroutines are made freely available at https://gitlab.com/dhamil/r2scan-subroutines. The data that support the findings of this study are available from the corresponding author upon reasonable request.

REFERENCES

[1] J. P. Perdew and K. Schmidt, AIP Conf. Proc. **577**, 1 (2001).
[2] A. D. Becke, Int. J. Quantum Chem. **23**, 1915 (1983).
[3] A. D. Becke and M. R. Roussel, Phys. Rev. A **39**, 3761 (1989).
[4] J. P. Perdew, Phys. Rev. Lett. **55**, 1665 (1985); **55**, 2370 (1985).
[5] J. Sun, A. Ruzsinszky, and J. P. Perdew, Phys. Rev. Lett. **115**, 036402 (2015).
[6] P. D. Mezei, G. I. Csonka, and M. Kallay, J. Chem. Theory Comput. **14**, 2469 (2018).
[7] T. Aschebrock and S. Kümmel, Phys. Rev. Res. **1**, 033082 (2019).
[8] B. Neupane, H. Tang, N. K. Nepal, S. Adhikari, and A. Ruzsinszky, Phys. Rev. Mater. **5**, 063803 (2021).
[9] D. A. Kitchaev, H. Peng, Y. Liu, J. Sun, J. P. Perdew, and G. Ceder, Phys. Rev. B **93**, 045132 (2016).
[10] J. Sun, R. C. Remsing, Y. Zhang, Z. Sun, A. Ruzsinszky, H. Peng, Z. Yang, A. Paul, U. Waghmare, X. Wu, M. L. Klein, and J. P. Perdew, Nat. Chem. **8**, 831 (2016).
[11] Z.-h. Yang, H. Peng, J. Sun, and J. P. Perdew, Phys. Rev. B **93**, 205205 (2016).
[12] I. G. Buda, C. Lane, B. Barbiellini, A. Ruzsinszky, J. Sun, and A. Bansil, Sci. Rep. **7**, 44766 (2017).
[13] H. Peng and J. P. Perdew, Phys. Rev. B **96**, 100101(R) (2017).
[14] Y. Zhang, J. Sun, J. P. Perdew, and X. Wu, Phys. Rev. B **96**, 035143 (2017).
[15] M. Chen, H.-Y. Ko, R. C. Remsing, M. F. Calegari Andrade, B. Santra, Z. Sun, A. Selloni, R. Car, M. L. Klein, J. P. Perdew, and X. Wu, Proc. Natl. Acad. Sci. U. S. A. **114**, 10846 (2017).
[16] A. Patra, J. E. Bates, J. Sun, and J. P. Perdew, Proc. Natl. Acad. Sci. U. S. A. **114**, E9188 (2017).
[17] R. C. Remsing, M. L. Klein, and J. Sun, Phys. Rev. B **96**, 024203 (2017).
[18] C. Shahi, J. Sun, and J. P. Perdew, Phys. Rev. B **97**, 094111 (2018).
[19] M. F. Calegari Andrade, H.-Y. Ko, R. Car, and A. Selloni, J. Phys. Chem. Lett. **9**, 6716 (2018).
[20] J. W. Furness, Y. Zhang, C. Lane, I. G. Buda, B. Barbiellini, R. S. Markiewicz, A. Bansil, and J. Sun, Commun. Phys. **1**, 11 (2018).
[21] C. Lane, J. W. Furness, I. G. Buda, Y. Zhang, R. S. Markiewicz, B. Barbiellini, J. Sun, and A. Bansil, Phys. Rev. B **98**, 125140 (2018).
[22] G. Sai Gautam and E. A. Carter, Phys. Rev. Mater. **2**, 095401 (2018).
[23] Y. Zhang, D. A. Kitchaev, J. Yang, T. Chen, S. T. Dacek, R. A. Sarmiento-Pérez, M. A. L. Marques, H. Peng, G. Ceder, J. P. Perdew, and J. Sun, npj Comput. Mater. **4**, 9 (2018).
[24] Y. Zhang, J. W. Furness, B. Xiao, and J. Sun, J. Chem. Phys. **150**, 014105 (2019).
[25] Y. Zhang, C. Lane, J. W. Furness, B. Barbiellini, J. P. Perdew, R. S. Markiewicz, A. Bansil, and J. Sun, Proc. Natl. Acad. Sci. U. S. A. **117**, 68 (2020).
[26] A. Pulkkinen, B. Barbiellini, J. Nokelainen, V. Sokolovskiy, D. Baigutlin, O. Miroshkina, M. Zagrebin, V. Buchelnikov, C. Lane, R. S. Markiewicz, A. Bansil, J. Sun, K. Pussi, and E. Lähderanta, Phys. Rev. B **101**, 075115 (2020).
[27] R. Wang, V. Carnevale, M. L. Klein, and E. Borguet, J. Phys. Chem. Lett. **11**, 54 (2020).
[28] R. Zhang, B. Singh, C. Lane, J. Kidd, Y. Zhang, B. Barbiellini, R. S. Markiewicz, A. Bansil, and J. Sun, arXiv:2003.11052 [cond-mat.str-el] (2020).

[29]Y. Zhang, J. Furness, R. Zhang, Z. Wang, A. Zunger, and J. Sun, Phys. Rev. B **102**, 045112 (2020).
[30]M. J. Mehl, M. Ronquillo, D. Hicks, M. Esters, C. Oses, R. Friedrich, A. Smolyanyuk, E. Gossett, D. Finkenstadt, and S. Curtarolo, Phys. Rev. Mater. **5**, 083608 (2021).
[31]J. Ning, J. W. Furness, and J. Sun, arXiv:2107.11850 [cond-mat.mtrl-sci] (2021).
[32]K. Pokharel, C. Lane, J. W. Furness, R. Zhang, J. Ning, B. Barbiellini, R. S. Markiewicz, Y. Zhang, A. Bansil, and J. Sun, arXiv:2004.08047 [cond-mat.supr-con] (2021).
[33]A. P. Bartók and J. R. Yates, J. Chem. Phys. **150**, 161101 (2019).
[34]J. W. Furness and J. Sun, Phys. Rev. B **99**, 041119 (2019).
[35]D. Mejía-Rodríguez and S. B. Trickey, J. Chem. Phys. **151**, 207101 (2019).
[36]A. P. Bartók and J. R. Yates, J. Chem. Phys. **151**, 207102 (2019).
[37]J. W. Furness, A. D. Kaplan, J. Ning, J. P. Perdew, and J. Sun, J. Phys. Chem. Lett. **11**, 8208 (2020).
[38]D. Mejía-Rodríguez and S. B. Trickey, Phys. Rev. B **102**, 121109(R) (2020).
[39]D. Mejía-Rodríguez and S. B. Trickey, J. Phys. Chem. A **124**, 9889 (2020).
[40]S. Ehlert, U. Huniar, J. Ning, J. W. Furness, J. Sun, A. D. Kaplan, J. P. Perdew, and J. G. Brandenburg, J. Chem. Phys. **154**, 061101 (2021).
[41]S. Grimme, A. Hansen, S. Ehlert, and J.-M. Mewes, J. Chem. Phys. **154**, 064103 (2021).
[42]J. P. Perdew, K. Burke, and M. Ernzerhof, Phys. Rev. Lett. **77**, 3865 (1996).
[43]L. Goerigk, A. Hansen, C. Bauer, S. Ehrlich, A. Najibi, and S. Grimme, Phys. Chem. Chem. Phys. **19**, 32184 (2017).
[44]G. Santra and J. M. L. Martin, J. Chem. Theory Comput. **17**, 1368–1379 (2021).
[45]S. Song, S. Vuckovic, E. Sim, and K. Burke, J. Phys. Chem. Lett. **12**, 800 (2021).
[46]S. Dasgupta, E. Lambros, J. P. Perdew, and F. Paesani, Nat. Commun. **12**, 6359 (2021).
[47]G.-X. Zhang, A. M. Reilly, A. Tkatchenko, and M. Scheffler, New J. Phys. **20**, 063020 (2018).
[48]S. Dick and M. Fernandez-Serra, Phys. Rev. B **104**, L161109 (2021).
[49]D. J. Tozer, V. E. Ingamells, and N. C. Handy, J. Chem. Phys. **105**, 9200 (1996).
[50]J. Kirkpatrick, B. McMorrow, D. H. P. Turban, A. L. Gaunt, J. S. Spencer, A. G. D. G. Matthews, A. Obika, L. Thiry, M. Fortunato, D. Pfau, L. Castellanos, S. Petersen, A. W. R. Nelson, P. Kohli, P. Mori-Sánchez, D. Hassabis, and A. J. Cohen, Science **374**, 1385 (2021).
[51]J. P. Perdew, Science **374**, 1322 (2021).
[52]J. P. Perdew, R. G. Parr, M. Levy, and J. L. Balduz, Jr., Phys. Rev. Lett. **49**, 1691 (1982).
[53]A. J. Cohen, P. Mori-Sánchez, and W. Yang, J. Chem. Phys. **129**, 121104 (2008).
[54]A. D. Becke and K. E. Edgecombe, J. Chem. Phys. **92**, 5397 (1990).
[55]A. Ruzsinszky, J. Sun, B. Xiao, and G. I. Csonka, J. Chem. Theory Comput. **8**, 2078 (2012).
[56]J. Sun, B. Xiao, and A. Ruzsinszky, J. Chem. Phys. **137**, 051101 (2012).
[57]J. Sun, B. Xiao, Y. Fang, R. Haunschild, P. Hao, A. Ruzsinszky, G. I. Csonka, G. E. Scuseria, and J. P. Perdew, Phys. Rev. Lett. **111**, 106401 (2013).
[58]J. W. Furness, N. Sengupta, J. Ning, A. Ruzsinszky, and J. Sun, J. Chem. Phys. **152**, 244112 (2020).
[59]M. Levy and J. P. Perdew, Phys. Rev. A **32**, 2010 (1985).
[60]M. Levy, Int. J. Quantum Chem. **36**, 617 (1989).
[61]M. Levy, Phys. Rev. A **43**, 4637 (1991).
[62]M. Levy and J. P. Perdew, Phys. Rev. B **48**, 11638 (1993).
[63]A. Görling and M. Levy, Phys. Rev. A **45**, 1509 (1992).
[64]L. Pollack and J. P. Perdew, J. Phys.: Condens. Matter **12**, 1239 (2000).
[65]L. Chiodo, L. A. Constantin, E. Fabiano, and F. Della Sala, Phys. Rev. Lett. **108**, 126402 (2012).
[66]J. P. Perdew, A. Ruzsinszky, J. Sun, and K. Burke, J. Chem. Phys. **140**, 18A533 (2014).
[67]E. Clementi and C. Roetti, At. Data Nucl. Data Tables **14**, 177 (1974).
[68]J. W. Furness and S. Lehtola, "Hartree–Fock orbitals for spherical atoms—A Python toolbox," code repository available at https://github.com/JFurness1/AtomicOrbitals.
[69]L. Kleinman and S. Lee, Phys. Rev. B **37**, 4634 (1988).
[70]P. S. Svendsen and U. von Barth, Int. J. Quantum Chem. **56**, 351 (1995).
[71]P. S. Svendsen and U. von Barth, Phys. Rev. B **54**, 17402 (1996).
[72]J. P. Perdew, S. Kurth, A. Zupan, and P. Blaha, Phys. Rev. Lett. **82**, 2544 (1999).
[73]S.-K. Ma and K. A. Brueckner, Phys. Rev. **165**, 18 (1968).
[74]Y. Wang and J. P. Perdew, Phys. Rev. B **43**, 8911 (1991).
[75]J. Sun, J. P. Perdew, and A. Ruzsinszky, Proc. Natl. Acad. Sci. U. S. A. **112**, 685 (2015).
[76]J. P. Perdew and Y. Wang, Phys. Rev. B **45**, 13244 (1992).
[77]A. D. Becke, Phys. Rev. A **38**, 3098 (1988).
[78]S. J. Chakravorty, S. R. Gwaltney, and E. R. Davidson, Phys. Rev. A **47**, 3649 (1993).
[79]S. P. McCarthy and A. J. Thakkar, J. Chem. Phys. **134**, 044102 (2011).
[80]L. A. Constantin, J. M. Pitarke, J. F. Dobson, A. Garcia-Lekue, and J. P. Perdew, Phys. Rev. Lett. **100**, 036401 (2008); J. M. Pitarke and A. G. Eguiliuz, Phys. Rev. B **63**, 045116 (2001)
[81]N. D. Lang and W. Kohn, Phys. Rev. B **1**, 4555 (1970).
[82]K. Patkowski, G. Murdachaew, C.-M. Fou, and K. Szalewicz, Mol. Phys. **103**, 2031 (2005).
[83]L. A. Curtiss, K. Raghavachari, P. C. Redfern, and J. A. Pople, J. Chem. Phys. **112**, 7374 (2000).
[84]P. Jurečka, J. Šponer, J. Černý, and P. Hobza, Phys. Chem. Chem. Phys. **8**, 1985 (2006).
[85]Y. Zhao, N. González-García, and D. G. Truhlar, J. Phys. Chem. A **109**, 2012 (2005).
[86]J. Sun, M. Marsman, G. I. Csonka, A. Ruzsinszky, P. Hao, Y. S. Kim, G. Kresse, and J. P. Perdew, Phys. Rev. B **84**, 035117 (2011).
[87]V. N. Staroverov, G. E. Scuseria, J. Tao, and J. P. Perdew, Phys. Rev. B **69**, 075102 (2004).
[88]P. Hao, Y. Fang, J. Sun, G. I. Csonka, P. H. T. Philipsen, and J. P. Perdew, Phys. Rev. B **85**, 014111 (2012).
[89]F. Tran, J. Stelzl, and P. Blaha, J. Chem. Phys. **144**, 204120 (2016).
[90]R. Kingsbury, A. Gupta, C. J. Bartel, J. M. Munro, S. Dwaraknath, M. Horton, and K. A. Persson, chemRxiv:10.33774/chemrxiv-2021-gwm9m-v2 (2021).
[91]A. D. Kaplan, B. Santra, P. Bhattarai, K. Wagle, S. T. u. R. Chowdhury, P. Bhetwal, J. Yu, H. Tang, K. Burke, M. Levy, and J. P. Perdew, J. Chem. Phys. **153**, 074114 (2020).
[92]M. G. Medvedev, I. S. Bushmarinov, J. Sun, J. P. Perdew, and K. A. Lyssenko, Science **355**, 49 (2017).